Noise Removal Using Factor Analysis of Dynamic Structures: Application to Cardiac Gated Studies

Philippe P. Bruyant, Jacques Sau and Jean-Jacques Mallet

Nuclear Spectroscopy and Image Processing Research Group, Biophysics Laboratory, Claude Bernard University, Lyon, France

Factor analysis of dynamic structures (FADS) facilitates the extraction of relevant data, usually with physiologic meaning, from a dynamic set of images. The result of this process is a set of factor images and curves plus some residual activity. The set of factor images and curves can be used to retrieve the original data with reduced noise using an inverse factor analysis process (iFADS). This improvement in image quality is expected because the inverse process does not use the residual activity, assumed to be made of noise. The goal of this work is to quantitate and assess the efficiency of this method on gated cardiac images. **Methods:** A computer simulation of a planar cardiac gated study was performed. The simulated images were added with noise and processed by the FADS-iFADS program. The signal-to-noise ratios (SNRs) were compared between original and processed data. Planar gated cardiac studies from 10 patients were tested. The data processed by FADS-iFADS were subtracted to the original data. The result of the substraction was studied to evaluate its noisy nature. **Results:** The SNR is about five times greater after the FADS-iFADS process. The difference between original and processed data is noise only, i.e., processed data equals original data minus some white noise. **Conclusion:** The FADS-iFADS process is successful in the removal of an important part of the noise and therefore is a tool to improve the image quality of cardiac images. This tool does not decrease the spatial resolution (compared with smoothing filters) and does not lose details (compared with frequential filters). Once the number of factors is chosen, this method is not operator dependent.

Key Words: factor analysis of dynamic structures; image processing; noise; gated cardiac images

J Nucl Med 1999; 40:1676–1682

Factor analysis of dynamic structures (FADS) can be used in nuclear medicine to account for spatial distribution and the temporal evolution of dynamic data. The result of FADS is a set of static factor images, each associated with a temporal curve called a factor (*1,2*). A factor image with its factor usually can be related to an anatomic and functional structure by an expert. Some of the studies using FADS rely on the interpretation of the factor images and factors (*3–5*), but a next step can be performed after FADS. The result of FADS can be used to retrieve most of the original dynamic data using the inverse FADS (iFADS) process. This is possible because the results of FADS almost contain the same amount of information as the original dynamic data, but the information is stored in a different way. The spatial information is in factor images, and the temporal information is described by factors. FADS-iFADS allows the retrieval of "pure" time-activity curves or images (*6–8*). iFADS also can be used as a highly efficient but lossy compression-decompression process because the factor images and curves are condensed forms of the raw data. This method has been proposed to save space on storage system (*9*). The third application is the removal of some noise by reconstructing the raw data using only the significant components. Very few nuclear medicine studies have used this last application (*10,11*), and, to our knowledge, no studies have been undertaken to quantitate such a method in terms of the signal-to-noise ratio (SNR).

In this study, the ability of the FADS-iFADS process to improve the image quality is quantitated on simulated images, for which the SNR is known. The FADS-iFADS process is also applied to clinical data, such as planar gated cardiac images, and the difference between the raw and processed data is studied to assess its noisy nature.

METHODS

Phantom Studies

The FADS-iFADS process was tested first by means of a computer simulation. Three factors were used to account for the data in the whole matrix (*2,4*). The atrial, ventricular and vascular factors and their corresponding curves were created numerically (Fig. 1). They were used with the iFADS program to build the model images. Then, to obtain a set of data well suited to our demonstration, Poisson and Gaussian noises were added to take into account the random nature of the radioactive disintegrations and the noise introduced by the imaging system, respectively. The additions of both noises were repeated 500 times, and the 500 sets of images obtained were summed to simulate the data acquired during 500 cardiac cycles.

Home-made programs generated a series of random values for each pixel using the random number generator of the computer. For the Poisson generator, the larger the series, the better the counting statistics. Once the number of cardiac cycles was chosen, the intensity of the Poisson noise was determined fully. Here, this number equaled 500.

The second home-made program generated a Gaussian noise that was added equally to all the pixels, independently of their intensity. This Gaussian noise had a mean value of 0. The level of noise in the images was determined by the dispersion of the random

Received Sep. 10, 1998; revision accepted Mar. 19, 1999.

For correspondence or reprints contact: P. Bruyant, PhD, Biophysics Laboratory 10, avenue Rockefeller 69373, Lyon cedex 08, France.

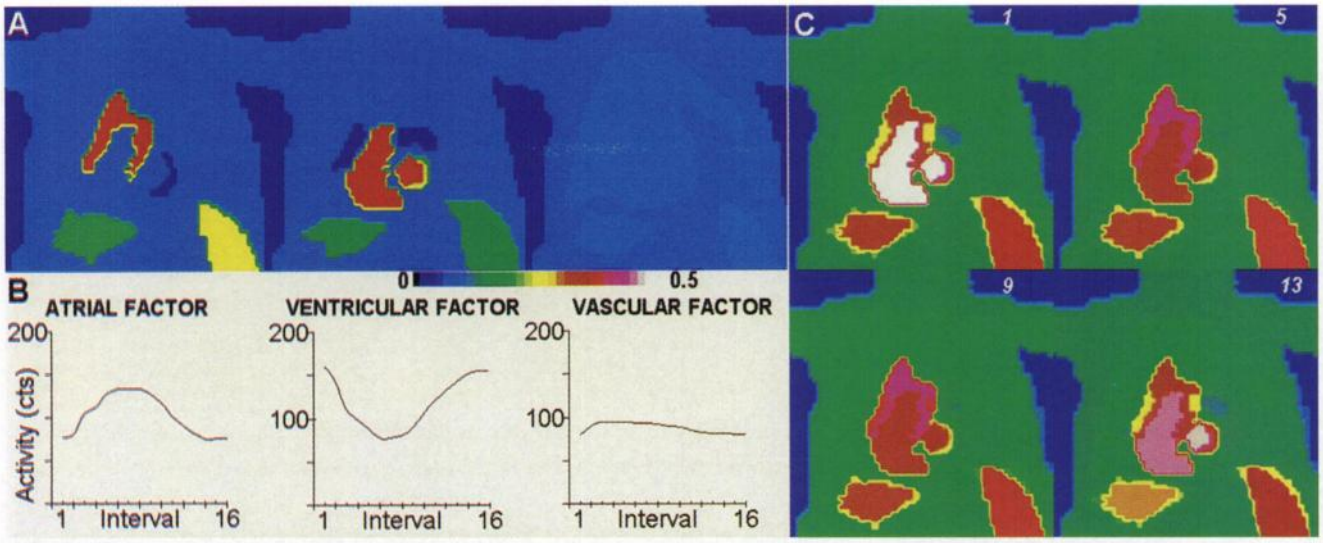

FIGURE 1. Factor images and curves used for simulation purposes. Relative intensities in images and shapes of curves are chosen to be comparable with normal clinical data. Image factors (A), with corresponding curves (B), are used by iFADS program to build 16 images of cardiac cycle. Only 4 images of cardiac cycle (intervals 1, 5, 9 and 13) are displayed in (C).

values, which was quantitated by the SD. Four values for the SD were tested (0.5, 0.75, 1.00 and 1.25 count per pixel). Because only integer values have physical meanings, the floating values returned by the noise generator programs were rounded to the nearest integer. The maximum pixel intensity in the model image before noise addition was set between 0 and 1 to obtain a maximal activity of approximately 500 counts per pixel in the images after the 500 iterations.

Patients

The study included 10 patients (7 men, 3 women; age 58 ± 10 y) directed to our department after myocardial infarction. The patients were chosen randomly among patients examined daily. No additional a priori criteria were used to select the patients.

Image Acquisition

Each patient received 740 MBq (20 mCi) ^{99m}Tc-pyrophosphate as a bolus injection. Image acquisition was performed on a Prism 2000XP dual-head gamma camera (Picker International, Inc., Cleveland, OH) using low-energy, high-resolution parallel collimators. Sixteen images per cardiac cycle were acquired over 500 cycles. Left anterior oblique images (64 × 64 pixels) were obtained, and the mean total counts per examination was 5932 ± 1351 kcts.

The terms "raw images," "simulated images" and "processed images" as used here refer to the raw clinical data, the simulated images after noise addition and the images resulting from the FADS-iFADS process, respectively.

Image Processing

FADS and iFADS were performed with home-made programs written in the C programming language and fully integrated in the Picker graphic environment, on a DEC Alpha computer (Digital Equipment Corp., Maynard, MA).

FADS Computing. The FADS program was applied to the raw and simulated images using three factors based on an original iterative method. Note that the following method does not follow the algorithm described by Barber (*1*) and Di Paola et al. (*2*).

Designating A as the original image data presented under a matrix form, then A is of dimensions (n,p), where n is the number of pixels (X matrix size × Y matrix size) and the integer p is the number of measurements (here, the number of intervals). FADS gives the i^{th} factor images (F_i) and curves (C_i), with i varying between 1 and the number of factors (q), to yield the following equation:

$$A = \sum_{i=1}^{q} F_i \times C_i + R, \qquad \text{Eq. 1}$$

where × denotes the matrix multiplication operator. For the sake of simplicity, F × C denotes the sum $\Sigma_{i=1}^{q} F_i \times C_i$. The matrix R is the part of the data not described by the factors.

Our iterative method for FADS is as follows. At the first iteration, the matrix $F^{(1)}$ is filled with random values. The matrix C is obtained using the formula:

$$C^{(1)} = \tilde{F}^{-1(1)} \times A, \qquad \text{Eq. 2}$$

where $\tilde{F}^{-1(1)}$ is the pseudo-inverse of $F^{(1)}$. The negative elements of C are set to 0.

Then, $F^{(2)}$ is obtained by the same procedure:

$$F^{(2)} = A \times \tilde{C}^{-1(1)}, \qquad \text{Eq. 3}$$

where $\tilde{C}^{-1(1)}$ is the pseudo-inverse of C. This procedure is repeated, and at each iteration r the norm (n) of the matrix:

$$R = (A - F^{(r)} \times C^{(r)}) \qquad \text{Eq. 4}$$

is computed, i.e.:

$$n = \|R\| = \|A - F^{(r)} \times C^{(r)}\|, \qquad \text{Eq. 5}$$

until n reaches a user-defined minimum.

In the factor images, the floating values are comprised between 0 and 1, but to be displayed, they are scaled to a 0–4095 interval and rounded.

iFADS Computing. The three factor images with their factors then are used by iFADS in the summation of the matrix products of each image factor by its corresponding curve. The previously defined F_i are of dimensions n,1 and the C_i are of dimensions 1,p.

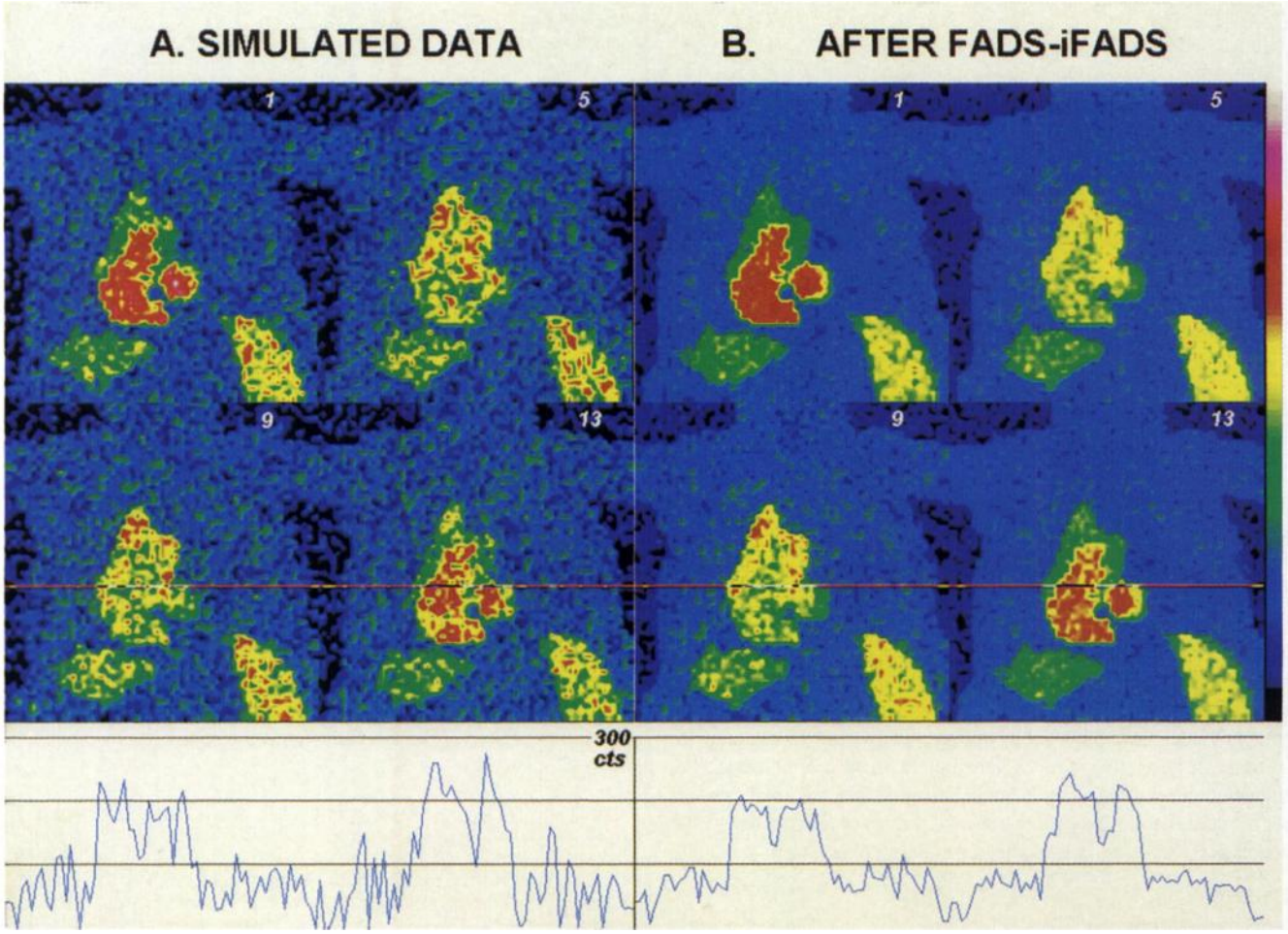

FIGURE 2. Results of factor analysis of dynamic structures-inverse FADS (FADS-iFADS) process on simulated images (intervals 1, 5, 9 and 13 are displayed here). (A) Simulated data are obtained from model data (see Fig. 1) after addition of Poisson noise and Gaussian noise with mean of 0 and SD = 1.25 cts/pixel. (B) After FADS-iFADS process, edges of structures are better defined. Although process image appears smoother, note that details are still visible. Activity profile (corresponding to red line on images 9 and 13) at bottom shows that contrast between regions of high and low activities is maintained, and all regions appear more homogeneous.

The matrix product $F_i \times C_i$ represents the amount of radioactivity corresponding to the i^{th} factor.

The matrix A′ is defined as:

$$A' = \sum_{i=1}^{q} F_i \times C_i \qquad \text{Eq. 6}$$

and is the raw data A minus residual activity.

Signal-to-Noise Ratio. For phantom data, the SNR of the simulated and processed images is assessed for each level of noise and is computed as follows:

$$SNRn = \frac{\sum_{k=0}^{p-1}\sum_{i=0}^{a-1}\sum_{j=0}^{b-1} M_{i,j,k}^2}{\sum_{k=0}^{p-1}\sum_{i=0}^{a-1}\sum_{j=0}^{b-1} (M_{i,j,k} - N_{i,j,k})^2}, \qquad \text{Eq. 7}$$

$$SNRp = \frac{\sum_{k=0}^{p-1}\sum_{i=0}^{a-1}\sum_{j=0}^{b-1} M_{i,j,k}^2}{\sum_{k=0}^{p-1}\sum_{i=0}^{a-1}\sum_{j=0}^{b-1} (M_{i,j,k} - P_{i,j,k})^2}, \qquad \text{Eq. 8}$$

where SNRn and SNRp represent the SNR corresponding to the simulated and processed images, respectively; p, a and b are the number of intervals, the width and the height of the image (in pixels), respectively; and $M_{i,j,k}$, $N_{i,j,k}$ and $P_{i,j,k}$ represent the value in pixel (i,j) at time k, in model, simulated and processed images, respectively.

Comparison of Raw and Processed Clinical Images

For clinical data, a pixel-by-pixel subtraction image is obtained. A Gaussian distribution of the values in the subtraction image would favor an image made of noise. For that reason, a Kolmogorov-Smirnov test is performed as follows. The histogram of the image is computed using 10 intervals; then, a home-made program fits the histogram with a Gaussian curve. The cumulative curves are computed from the histogram and the Gaussian curve. These curves, which look like two sigmoids, are normalized to 1, and one is subtracted from the other. The greatest difference is located in the Kolmogorov-Smirnov table. If the greatest absolute difference is smaller than a given value, then the two curves are not significantly different.

Temporal and Spatial Autocorrelation Functions. Autocorrelation functions are computed to show that the subtraction image contains white noise. The spatial autocorrelation looks for a

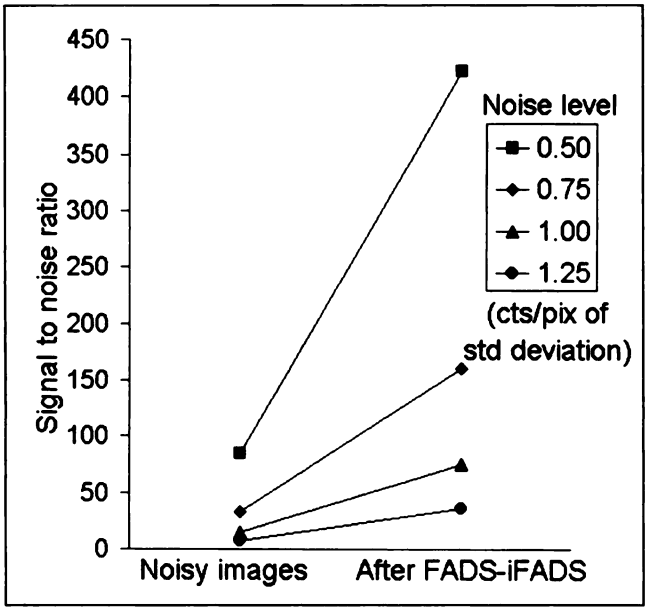

FIGURE 3. SNR increases for all tested levels of noise on simulated images. For each level of noise, SNR is about five times greater after factor analysis of dynamic structures-inverse FADS (FADS-iFADS) pix = pixel.

correlation between each pixel and its neighbors in the same image (i.e., at the same instant), and is computed as follows:

$$Cs_{i,j,k} = \sum_{i'=0}^{a-1-i} \sum_{j'=0}^{b-1-j} (A_{i',j',k} - \bar{A}_k) \times (A_{i'+i,j'+j,k} - \bar{A}_k), \quad \text{Eq. 9}$$

where $Cs_{i,j,k}$ is the spatial autocorrelation of pixel (i,j) at time k; a and b are the width and height of the image (in pixels), respectively; $A_{i',j',k}$ is the activity in the pixel (i',j') at time k; $\bar{A}_k$ is the arithmetic mean of image intensity at time:

$$\overline{A_k} = \frac{1}{ab}\left(\sum_{i=0}^{a-1} \sum_{j=0}^{b-1} A_{i,j,k}\right). \quad \text{Eq. 10}$$

The spatial correlation coefficient $Rs_{i,j,k}$ is obtained for each time k by dividing each value of $Cs_{i,j,k}$ by the maximum value:

$$Rs_{i,j,k} = \frac{1}{Cs_{0,0,k}} \times Cs_{i,j,k}. \quad \text{Eq. 11}$$

As in Barber (*1*) and Di Paola et al. (*2*), the term dixel (dynamic study pixel) represents the time-activity curve of a given pixel. The temporal autocorrelation looks for a correlation inside a given dixel. The mathematical formulas for autocorrelations are as

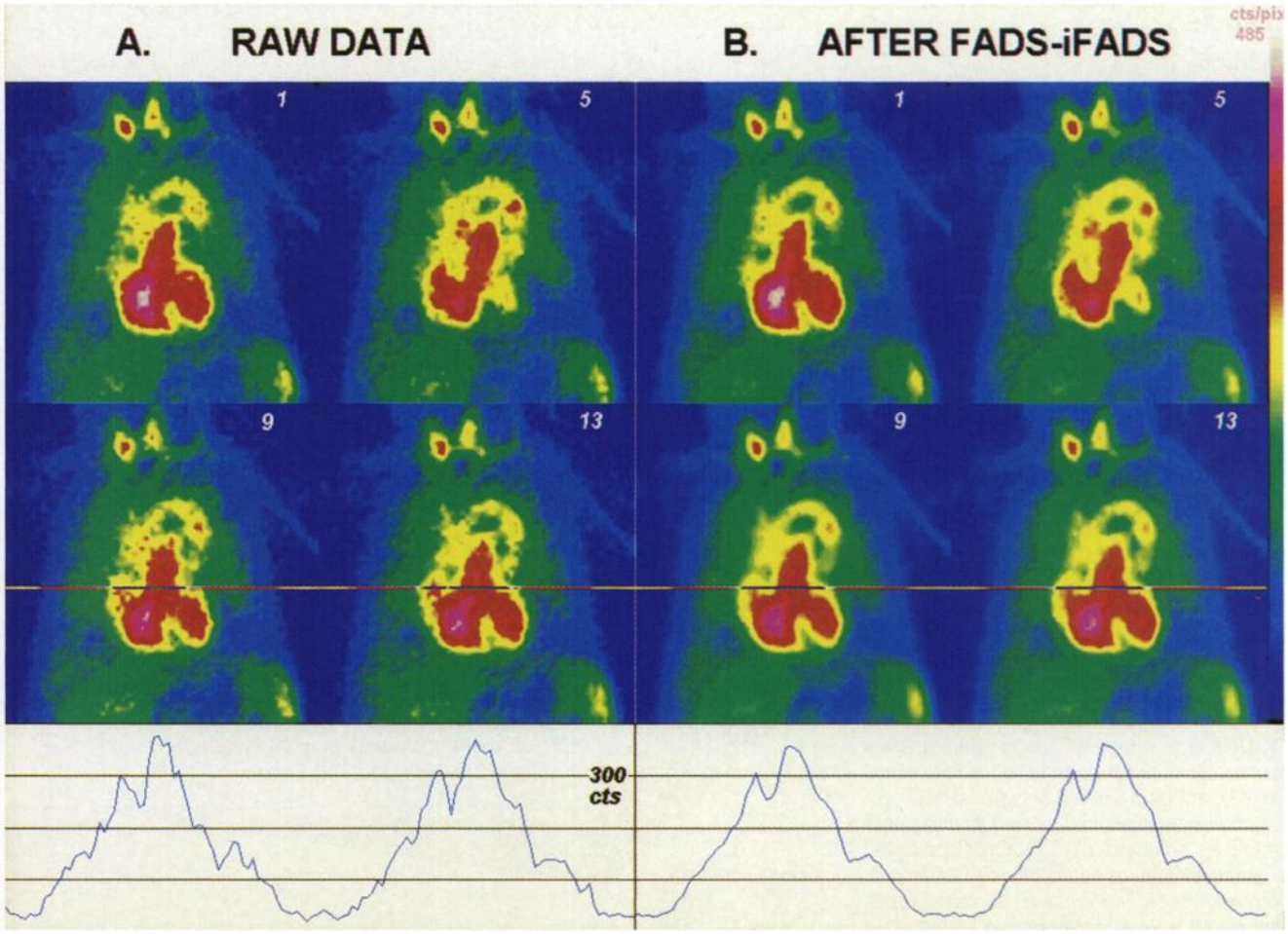

FIGURE 4. Result of factor analysis of dynamic structures-inverse FADS (FADS-iFADS) process on set of clinical images for one patient (only intervals 1, 5, 9 and 13 are displayed here). Processed images appear smoother and less granular, and contours are better defined. Activity profile (corresponding to red line on images 9 and 13) at bottom shows that, as in simulated images (Fig. 2), processed images lack speckles observed on raw data.

TABLE 1
Kolmogorov-Smirnov Test for Gaussian Distribution of Subtraction Images

Patient no.									
1	2	3	4	5	6	7	8	9	10
0.08801	0.06086	0.06194	0.06983	0.07526	0.05970	0.07471	0.06261	0.06594	0.08137

$P < 0.01$ for all values.

follows:

$$Ct_{i,j,k} = \sum_{k'=0}^{p-k-1} (A_{i,j,k'} - \bar{A}_{i,j}) \times (A_{i,j,(k'+k)} - \bar{A}_{i,j}), \quad \text{Eq. 12}$$

where $A_{i,j,k'}$ is the activity in the pixel (i,j) at the time k'; $\bar{A}_{i,j}$ is the arithmetic mean of intensity in pixel (i,j) in the course of time:

$$\overline{A_{i,j}} = \frac{1}{p}\left(\sum_{k=0}^{p-1} A_{i,j,k}\right). \quad \text{Eq. 13}$$

The temporal correlation coefficient $Rt_{i,j,k}$ is obtained for each pixel (i,j) by dividing the value of $Ct_{i,j,k}$ by the maximum value:

$$Rt_{i,j,k} = \frac{1}{Ct_{i,j,0}} \times Ct_{i,j,k}. \quad \text{Eq. 14}$$

RESULTS

Phantom Studies

A set of simulated images allowed estimation of the gain brought by the FADS-iFADS process qualitatively (Fig. 2) and quantitatively (Fig. 3). The SNR was about five times greater after processing.

Patient Studies

The processed data were compared with the raw data (Fig. 4). The Kolmogorov-Smirnov test confirmed the Gaussian nature of the distribution of the values in the subtraction image (processed image minus raw image) (Table 1). The spatial autocorrelation image visually confirmed that no correlation existed in the subtraction images (Fig. 5) between one pixel and its neighbors. By definition, the autocorrelation coefficient equaled 1 when a given pixel at a given interval was compared with itself. The largest correlation coefficient strictly lower than 1 equaled 0.08964 for the spatial autocorrelation (among all pixels over all images and all patients, except pixel [0,0]) (Table 2). The temporal autocorrelation function was used to look for a correlation between pixels of the same dixel. The first point of the

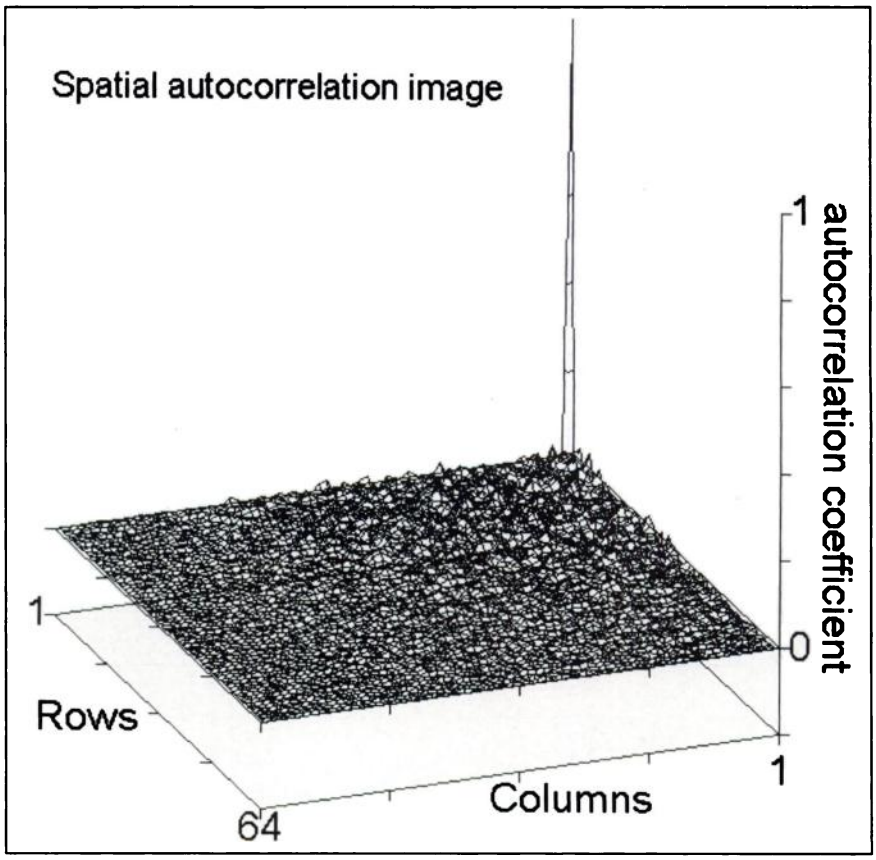

FIGURE 5. Image of spatial autocorrelation coefficients for patient 10 for first interval. If correlation existed between pixels (i,j) and their neighbors at (i+i', j+j'), then peak should be observed at (i',j'). Only one peak is clearly visible, at coordinates (0,0), which corresponds to correlation of each pixel with itself. Image is rather flat elsewhere, thereby indicating that no significant correlation exists between pixel and its close or far neighbors.

TABLE 2
Maximum Spatial Autocorrelation Coefficient Lower than 1

Patient no.									
1	2	3	4	5	6	7	8	9	10
−0.05878	−0.08918	−0.06379	−0.06535	−0.03417	−0.05982	−0.06031	0.08964	−0.06559	−0.06988

temporal function represented the correlation of each pixel with itself. Then, the i^{th} point represented the correlation of a pixel with the i^{th} pixel of the same dixel. We observed that the autocorrelation function was a Dirac function (Fig. 6); thus, the residual activity was almost white noise. Except for the first point, all values were between −0.17 and 0.02 in all patients. Such low values showed the absence of correlations. Because no spatial or temporal autocorrelations were evident, the subtraction images were made only of white noise.

DISCUSSION

In their study on myocardial blood flow, Wu et al. (*6*) used FADS to generate parametric images. They noticed a decrease in the noise level on these images but did not specifically address this observation. In this study, the ability of the FADS-iFADS process to improve image quality in gated planar cardiac studies was assessed quantitatively. The phantom study showed that the SNR was greatly enhanced, and the clinical study showed that only a white noise was subtracted from raw data, resulting in visually improved processed images.

By removing most of the speckles, the FADS-iFADS process enhanced the homogeneity between pixels containing equal amounts of radioactive tracer. This process is expected to be useful when applied before noise-sensitive methods, such as edge detection based on derivatives, or slope computing of time-activity curves. This study indicates that the FADS-iFADS process can be used for noise removal and also should be useful in removing undesirable data that could hide data of interest. This application has been used in neurophysiology, where artifacts caused by ocular movements have been removed successfully from electroencephalographic recordings (*12*) using principal components analysis.

Several methods currently are available for image restoration (i.e., for the minimization of the noise). One of the most common is the use of the Wiener filter (*13–15*), a band-pass filter intended to minimize both the noise (low-pass filter) and the blur (high-pass filter). With the method outlined in this study, however, no smoothing or decrease in spatial resolution was observed as a result of the SNR enhancement. Sophisticated approaches that enhance the SNR, such as the Bayesian estimation, use a priori information (Lorentzian or Gaussian distributions). Except for the number of factors, no hypothesis is required to use the FADS-iFADS method, and no assumptions are made about the nature of the noise to be removed. Once the number of factors is determined, the

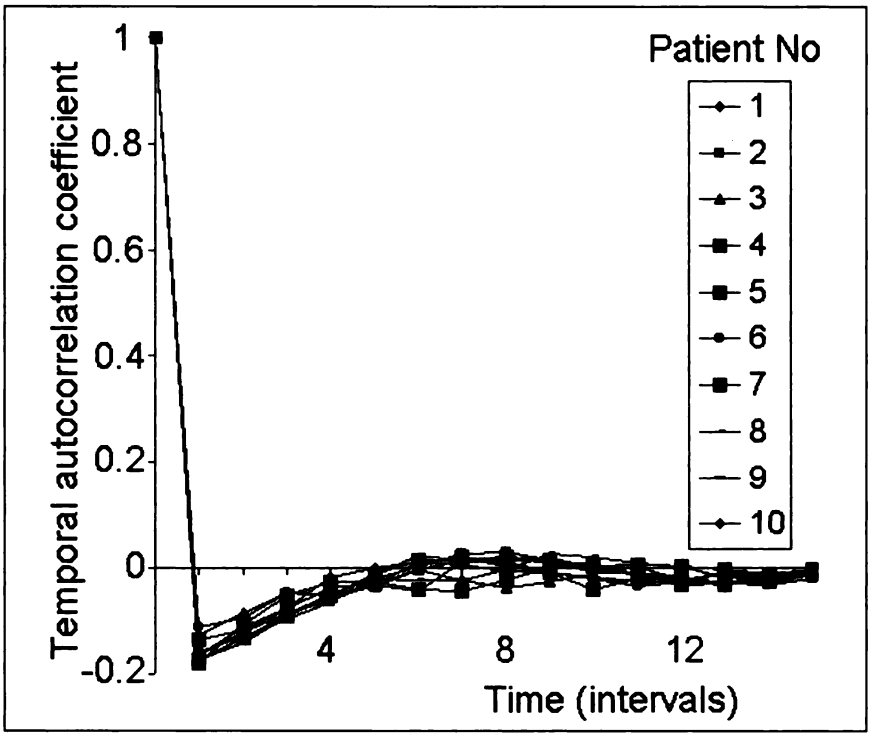

FIGURE 6. One temporal autocorrelation is computed for each of the 4096 dixels of subtraction image (processed data minus raw data) in each patient. These 4096 functions are averaged for each patient. Mean temporal autocorrelation functions are presented. Because functions rapidly decrease from 1, no significant temporal autocorrelation is seen.

process is completely operator independent and, on our computer, lasts less than 40 s with a set of sixteen 64 × 64 images.

The FADS-iFADS method uses the result of the FADS and iFADS but does not depend on the FADS algorithm. Therefore, it also should apply using the algorithm described by Barber (*1*) and DiPaola et al. (*2*). However, the method requires that true (unnormalized) values be obtained for factor images and curves.

CONCLUSION

This study emphasizes the potential use of the FADS-iFADS method for image quality improvement. The method is now being tested on dynamic studies in our department and should be especially interesting when applied to images with low activity, for example in the first phase of bone scintigraphy or in the vascular phase of renal scintigraphy.

REFERENCES

1. Barber DC. The use of principal components in the quantitative analysis of gamma camera dynamic studies. *Phys Med Biol.* 1980;25:283.
2. Di Paola R, Bazin JP, Aubry F, et al. Handling of dynamic sequences in nuclear medicine. *IEEE Trans Nucl Sci.* 1982;NS29:1310–1321.
3. Billotey C, Sarfati E, Aurengo A, et al. Advantages of SPECT in technetium-99m-sestamibi parathyroid scintigraphy. *J Nucl Med.* 1996;37:1773–1778.
4. Cavaillolès F, Bazin JP, Pavel D, et al. Comparison between factor analysis of dynamic structures and Fourier analysis in detection of segmental wall motion abnormalities: a clinical evaluation. *Int J Card Imaging.* 1995;11:263–272.
5. Edeline V, Frouin JP, Bazin JP, et al. Factor analysis as a means of determining response to chemotherapy in patients with osteogenic sarcoma. *Eur J Nucl Med.* 1993;20:1175–1185
6. Wu HM, Hoh CK, Buxton DB, et al. Quantification of myocardial blood flow using dynamic nitrogen-13-ammonia PET studies and factor analysis of dynamic structures. *J Nucl Med.* 1995;36:2087–2093.
7. Kakuta T, Suzuki Y, Hida M, et al. Functional evaluation of the remaining kidney in donors by radionuclide dynamic imaging using a graphic method with factor analysis. *Nucl Med Commun.* 1997;18:937–942.
8. Morvan D, Bazin JP, Cavailloles F, DiPaola R. Correction of scattering effects by factor analysis: a simulation of a clinical study. In: *Proceedings of the 25th Congress of the Society of Nuclear Medicine-Europe, Budapest, 1987.* Stuttgart, Germany: Schattauer Verlag; 1988:41–44.
9. Chameroy V, DiPaola R. High compression of nuclear medicine dynamic studies. *Int J Card Imaging.* 1990;5:261–269.
10. Wendt RE III, Murphy PH, Treffert JD, et al. Application and interpretation of principal components analysis of gated cardiac images [abstract]. *J Nucl Med.* 1993;34:843.
11. Moore WH, Treffert JD, Schneider PM, et al. Principal components analysis enhances the assessment of regional wall motion from cine display of gated blood pool [abstract]. *J Nucl Med.* 1995;36:512.
12. Lagerlund TD, Sharbrough FW, Busacker NE. Spatial filtering of multichannel electroencephalographic recordings through principal components analysis by singular value decomposition. *J Clin Neurophysiol.* 1997;14:73–82.
13. Miller TR, Goldman KJ, Epstein DM, et al. Improved interpretation of gated cardiac images by use of digital filters. *Radiology.* 1984;152:795–800.
14. Miller TR, Rollins ES. A practical method of image enhancement by interactive digital filtering. *J Nucl Med.* 1985;26:1075–1080.
15. King MA, Miller TR. Use of a nonstationary temporal Wiener filter in nuclear medicine. *Eur J Nucl Med.* 1985;10:458–461.